Polaron luminescence in iron-doped lithium niobate

Aïssa Harhira, Laurent Guilbert, P. Bourson, Hervé Rinnert

Polaron luminescence in iron-doped lithium niobate

A. Harhira, L. Guilbert, P. Bourson
Laboratoire Matériaux Optiques, Photonique et Systèmes, UMR CNRS 7132, University Paul Verlaine of Metz and Supélec, 2 rue E. Belin, 57070 Metz, France

H. Rinnert
Laboratoire de Physique des Matériaux, UMR CNRS 7556, Nancy, France

Abstract Photoluminescence related to the bound polaron Nb_{Li}^{4+} is investigated as a function of temperature and incident light intensity in iron-doped lithium niobate crystals with various iron concentrations. Experiments are done under constant-wave (CW) and pulsed illumination. Its found that the decay time is always monoexponential. The radiative lifetime, the activation energy of the nonradiative lifetime and the quenching temperature are only weakly sensitive to iron concentration. On the other hand, the magnitude of the photoluminescence signal seems strongly correlated to the Fe^{2+} concentration, and the superlinear regime evidenced at low CW illumination definitely confirms that polaron excitation in lithium niobate is a two-step process.

1 Introduction

Lithium niobate ($LiNbO_3$, LN) is of great interest for optical applications owing to its nonlinear and photorefractive properties. It is used either as bulk crystals or microstructures in a large variety of devices including lasers, electro-optic modulators, acousto-optic filters and holographic memories [1]. Precise knowledge of the light-induced properties of LN is of major importance for many applications. Most of these properties involved in device operation are sensitive to the concentration of point defects and to the reduction degree of the material. It is known that the intrinsic defective nature of LiNbO3 mainly consists of niobium ions in lithium sites (the so-called niobium antisites). The niobium antisite defect Nb_{Li}^{5+} is able to trap an electron on an energy level below the conduction band, giving a small bound polaron Nb_{Li}^{4+} [2]. This defect plays a major role in light-induced phenomena (photoconductivity, light-induced absorption and the pho-torefractive effect [3–5]). Some physical properties of this polaron, namely its broad absorption band peaking at 1.6 eV (740 nm) and the dependence of its lifetime on the distance to the nearest empty deep trap [6–8], have been described in the literature. Previous studies have also shown that excita-tion of congruent lithium niobate in the visible range always gives a photoluminescence (PL) band in the near infrared, which was attributed to the bound polaron Nb_{Li}^{4+} [9]. The PL band can be exploited to measure the chemical reduc-tion degree of the material. It has been shown by micro-photoluminescence (μ-PL) experiments that the neighborhood of titanium-diffused waveguides exhibits high PL contrast, which reflects the heterogeneous chemical reduction experienced by the sample during the annealing process of waveguide fabrication. More recently, the PL dynamics of undoped congruent LN has been measured versus temperature [10].

In this article, we present a more detailed experimen-tal investigation of the photoluminescence in iron-doped $LiNbO_3$. For the first time, both the magnitude of the PL signal and its decay time are studied as a function of the temperature, and the influence of the incident light intensity is also examined.

Table 1 Lithium content C_{Li}, total iron concentration C_{Fe} and concentration of Fe^{2+} ions $C_{Fe^{2+}}$ in the investigated samples. For LN:Fe 1% the value of C_{Fe} is the one measured by SIMS analysis at the surface of the diffused layer

Sample	C_{Li} (mol%)	C_{Fe} (10^{18} cm^{-3})	$C_{Fe^{2+}}$ (10^{18} cm^{-3})
LN:Fe 0.02% mol	48.64 ± 0.10	3.76	0.31
LN:Fe 0.05% mol	48.61 ± 0.10	9.40	0.87
LN:Fe 1% mol	48.58 ± 0.10	188	Unknown

2 Experimental methods

2.1 Crystals

Relevant parameters of the iron-doped LN samples are summarized in Table 1. In the first column, the Li concentration C_{Li} is determined by Raman measurements [11]. The first two samples LN:Fe 0.02% and LN:Fe 0.05% are cut from Czochralski crystals doped by adding Fe_2O_3 to the melt. A thermal annealing was made to increase the concentration of Fe^{2+} ions and absorption measurements were used to determine this concentration [12, 13]. The third sample LN:Fe 1% is not a bulk sample but a doped layer made by Fe diffusion. The total concentration of iron at the upper surface (1% mol) has been determined by SIMS (Secondary ion mass spectrometry) measurement.

2.2 Experimental setups

Two kinds of excitations were used: continuous-wave (CW) excitation at 633 nm by a He:Ne laser and pulse excitation by a frequency-doubled YAG:Nd laser at 532 nm. In both cases, the temperature was varied between 4 and 300 K. The sample was put in an optical cryostat equipped with silica glass windows. The cryostat was first cooled to 4 K and then heated step by step to 300 K. The temperature of the crystal holder was controlled with a typical accuracy of 0.2 K. The PL signal was collected at 90° from the incident light and was analyzed by a monochromator equipped with a 600 grooves/mm grating. The signal was detected by a photomultiplier tube cooled at 190 K.

For time-resolved measurements, the PL time response was usually re corded at 860 nm using a boxcar signal averager, after excitation by 532-nm laser pulses of 8-ns duration. The repetition rate was typically 10 Hz in all measurements. The spectral response of the detection system was accurately calibrated with a tungsten-wire calibration source.

Complementary measurements under CW illumination at 633 nm were done at room temperature at 633 nm using a Labram micro-spectrometer (Jobin Yvon) equipped with three objectives. The incident laser power was varied through three decades using attenuators of various optical densities. The light intensity was estimated by the ratio of the incident power to the spot area πw_0^2, with w_0 the radius at $1/e$, given by $w_0 = 0.61\lambda/(\text{N.A.})$ The numerical apertures (N.A.) of the objectives were 0.9, 0.6 and 0.25, respectively. The spectra were recorded from 1000 to 5000 cm^{-1} (relative shift from the exciting wavenumber) and it has been necessary to increase drastically the accumulation time in the low-intensity range (typically below 10 kW/cm^2, depending on samples) because of the weakness of the signal. A correcting factor was applied to the PL signal in order to account for these two different accumulation times. An overlap was taken between the two intensity ranges in order to adjust the correcting factor. It should be noticed that in this complementary study, the axis of the incident light beam was parallel to the crystal axis z for all samples. Polarization effects have not been studied. As concerns the gradually doped sample LN:Fe 1%, the light beam was focused near the surface of the iron-diffused layer, and the axial resolution (∼3 μm with a ×100 objective) was comparable to the depth of the doping profile at half maximum deduced from SIMS measurements (∼2.5 μm).

3 Experimental results

3.1 CW measurements

3.1.1 Temperature dependence

Figure 1 shows the PL spectra for LN:Fe 0.02% mol, 0.05% mol and 1% mol. The shape is similar for all samples, but LN:Fe 1% mol gives a much more intense signal. The PL spectrum consists of a broad Gaussian band peaking at ∼1.4 eV, with full width at half maximum (FWHM) about 130 nm (∼0.3 eV) at room temperature. The peak amplitude and the integrated area gradually increase at decreasing temperature down to 180 K, and then reach a quasi-constant value below 180 K. This classical behavior implies that different microscopic processes are involved in polaron relaxation: nonradiative processes are more efficient at room temperature, whereas radiative relaxation prevails below 180 K. It should be noticed that the complicated spectral shape of the PL band reported in previous work [9] was due to the fact that no calibration of the spectrometer was made.

In Fig. 2, the PL integrated area corrected from the background is plotted as a function of the reciprocal temperature. The data are taken for the three samples at the same pump power and they have been normalized to unity at low temperature (4 K). The dimensionless vertical unit thus represents the quantum efficiency of the PL process relative to its low-temperature limit. The thermal behavior of the Fe-doped crystals is similar to the one of undoped crystal [10]. The strong decrease of the PL signal observed above 180 K

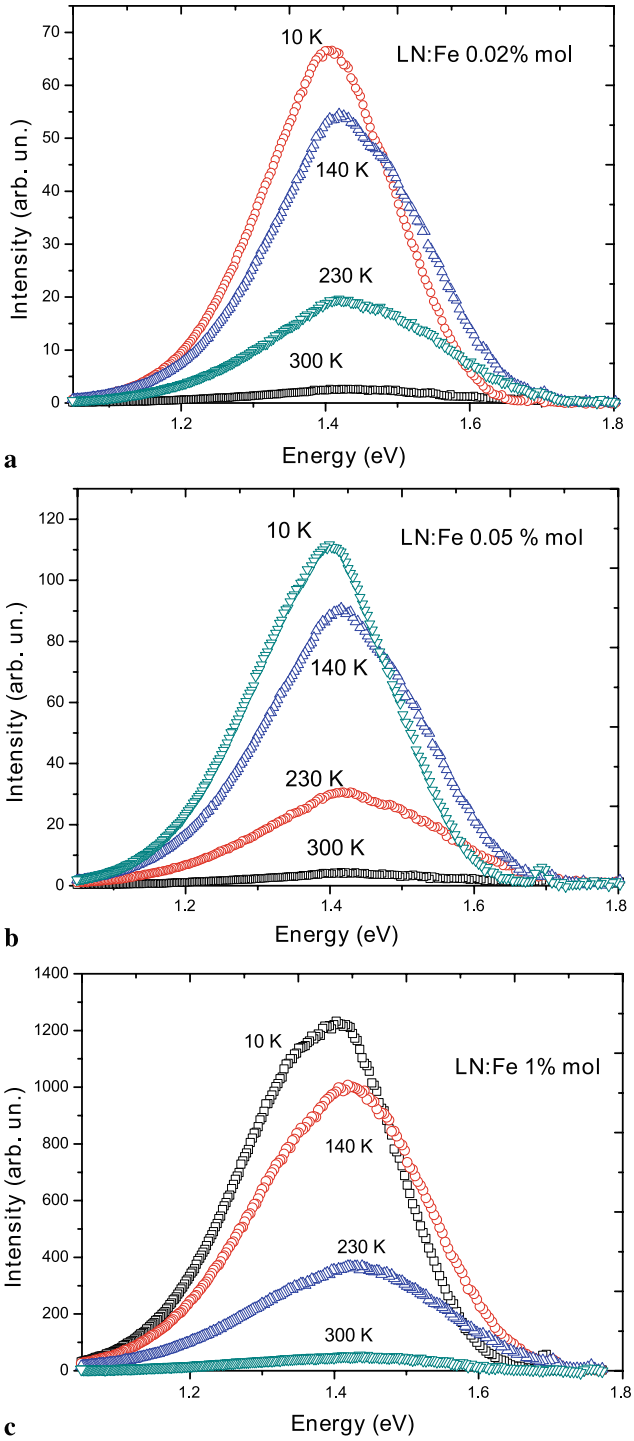

Fig. 1 Photoluminescence spectra for LN:Fe 0.02% mol (**a**), LN:Fe 0.05% mol (**b**) and LN:Fe 1% mol (**c**). The arbitrary unit is the same for the three graphs

can be described by an apparent activation energy. The PL intensity can be fitted with a sigmoidal function:

$$I_{\mathrm{PL}}(T) = \frac{I_0}{1 + C \times \exp(-E_{\mathrm{a}}/k_{\mathrm{B}}T)}, \tag{1}$$

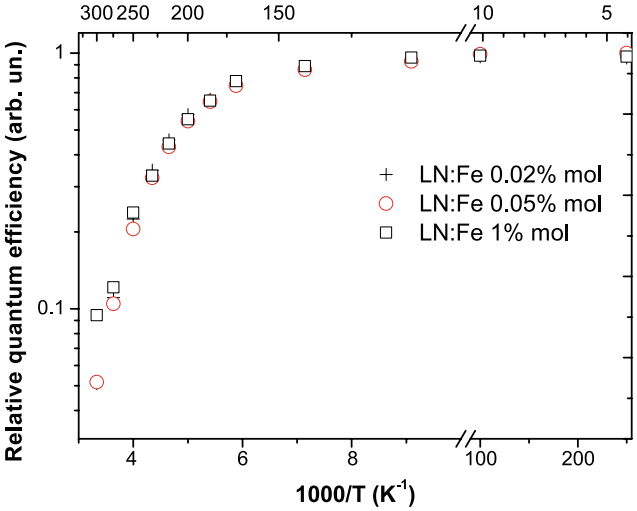

Fig. 2 Integrated area of the polaron band versus reciprocal temperature. The vertical unit (logarithmic scale) is normalized to the low-temperature limit, and thus corresponds to the quantum efficiency (assuming it tends to unity for $T \to 0$)

Table 2 Activation energy and quenching temperature obtained from least-square fits of the PL integrated area versus temperature, according to (1)

Sample	E_{a} (meV)	T_{Q} (K)
LN:Fe 0.02% mol	210 ± 20	190 ± 20
LN:Fe 0.05% mol	200 ± 20	190 ± 20
LN:Fe 1% mol	170 ± 30	170 ± 20
LN congruent [10]	220 ± 20	210 ± 20

with I_0 the PL intensity at low temperature, C a constant, E_{a} the activation energy, k_{B} the Boltzmann constant and T the absolute temperature. The quenching temperature T_{Q} can be defined by

$$I_{\mathrm{PL}}(T_{\mathrm{Q}}) = \frac{I_0}{2}. \tag{2}$$

A summary of the values obtained for the activation energy and the quenching temperature in the three samples is given in Table 2. An interpretation of (1) will be given in Sect. 3.2.1.

3.1.2 Dependence on incident intensity

In Fig. 3, the PL integrated area (corrected from the background) is shown in log–log scale as a function of the incident intensity ($\lambda_{\mathrm{exc}} = 633$ nm, $T = 293$ K). For all samples, the variation is clearly linear at high intensity (above $\sim$10 kW/cm^2), whereas a superlinear regime is observed at low intensity (below 2 kW/cm^2). For the highly doped sample (LN:Fe 1% mol), this superlinear regime is clearly

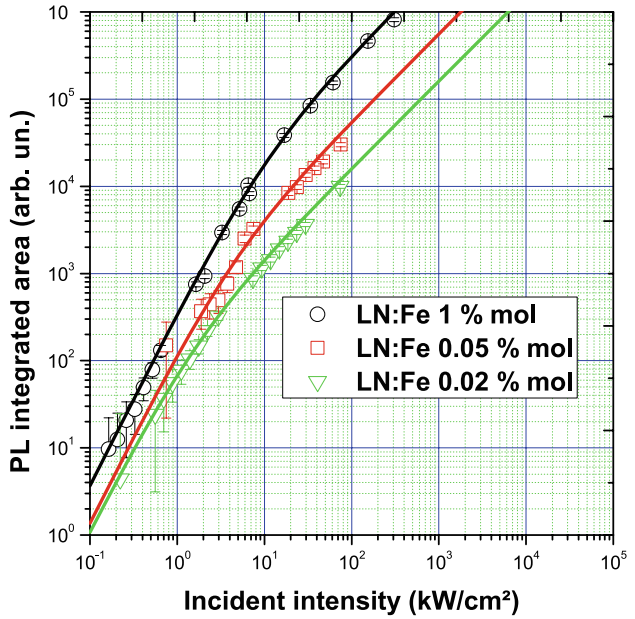

Fig. 3 Dependence of the PL integrated area on the incident CW intensity

Table 3 Fitting parameters of the PL integrated area versus incident intensity, according to (3)

Sample	A (arb. units)	I_{lin} (kW/cm^2)
LN:Fe 0.02% mol	160 ± 8	1 to 2
LN:Fe 0.05% mol	500 ± 25	3 to 5
LN:Fe 1% mol	3000 ± 150	8 to 10

quadratic. It is more difficult to determine the power law at low intensities for weakly doped samples (0.05% mol and 0.02% mol) because the signal is much weaker. If we assume that the superlinear regime is quadratic in all samples, the PL dependence can be fitted with an empirical function of the form

$$I_{\text{PL}}(I) = \frac{A \times I^2}{I + I_{\text{lin}}}, \tag{3}$$

with I_{lin} the threshold intensity of the linear regime and A a constant. These parameters depend on the doping level. The fits are shown by solid lines in Fig. 3. The fitting parameters are reported in Table 3.

3.2 Time-resolved measurements

3.2.1 Dependence on temperature

We have measured the time decay of the PL intensity at 860 nm in all samples at different temperatures and at different pulse energies. The results are shown in Fig. 4 for LN:Fe 0.05% mol. The PL intensities are normalized to the

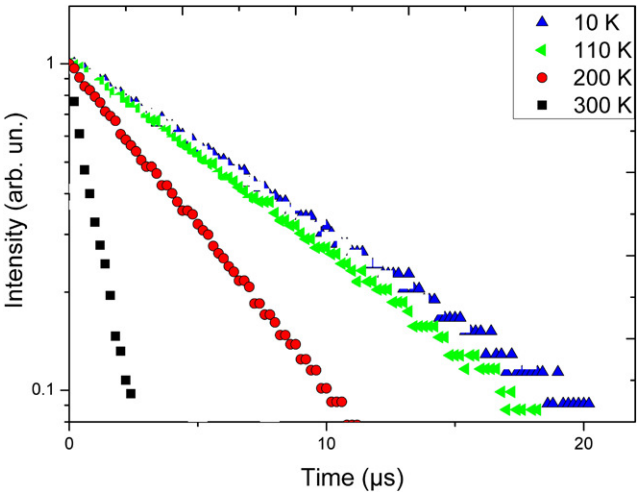

Fig. 4 Logarithmic plot of the photoluminescence decay at 860 nm after pulse excitation at 532 nm in LN:Fe 0.05% mol (normalized to the initial value)

initial value measured just after the pump pulse at $t \sim 0$. It should be noticed that the PL decays are monoexponential and insensitive to the emission wavelength in the whole range of the PL band (from 800 to 1000 nm). This suggests that only one radiative center is responsible for the PL signal under 532-nm excitation, contrary to what was previously observed under 355-nm excitation [10].

The results for the two other samples are not shown in the figure. They are very similar to those of LN:Fe 0.05% mol. Hence, in all samples the PL decay can be well fitted by a monoexponential function $I(t) = I(0)\exp(-t/\tau)$ with τ the decay time. At $T = 250$ K, the fitting values are $\tau = 2.3 \pm 0.1$ µs for LN:Fe 0.02% mol and 2.0 ± 0.1 µs for LN:Fe 0.05% mol.

The temperature dependence of the decay time is shown in Fig. 5. For temperatures below 180 K, the decay time is constant, $\sim 8.0 \pm 0.1$ µs for LN:Fe 0.02% mol and 8.2 ± 0.1 µs for LN:Fe 0.05% mol. These values can be considered as equal within experimental accuracy. The temperature dependence of the decay time fits well with a sigmoidal function:

$$\tau(T) = \frac{\tau_{\text{R}}}{1 + C \times \exp(-E_{\text{a}}/k_{\text{B}}T)}, \tag{4}$$

with τ_{R} the radiative lifetime corresponding to the low-temperature limit.

As for the temperature dependence of the PL intensity (see Sect. 3.1.1), a quenching temperature T_{Q} can be defined by $\tau(T_{\text{Q}}) = \tau_{\text{R}}/2$. The fitting parameters τ_{R}, E_{a} and T_{Q} are given in Table 4. The values of E_{a} and T_{Q} determined in this way are almost equal to those deduced from the thermal behavior of the integrated area (Table 2).

Finally, all experimental results are consistent with a classical relaxation scheme involving an athermal, radiative

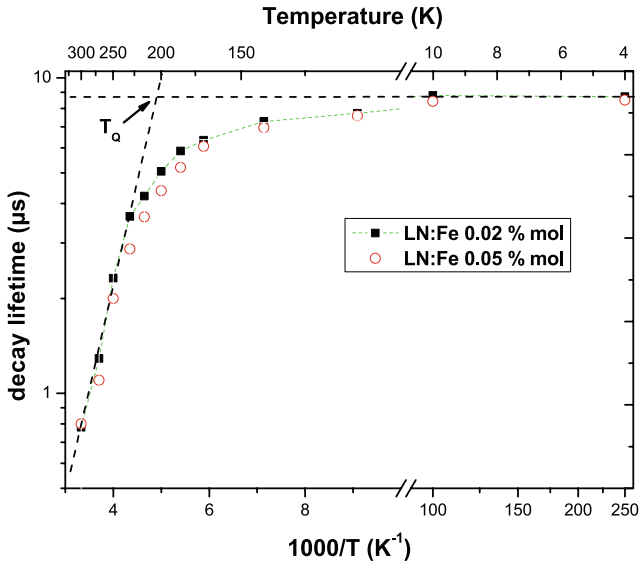

Fig. 5 Temperature dependence of photoluminescence decay time. The *dashed lines* represent the fitting function (4) and its asymptotic limits, for LN:Fe 0.02% mol

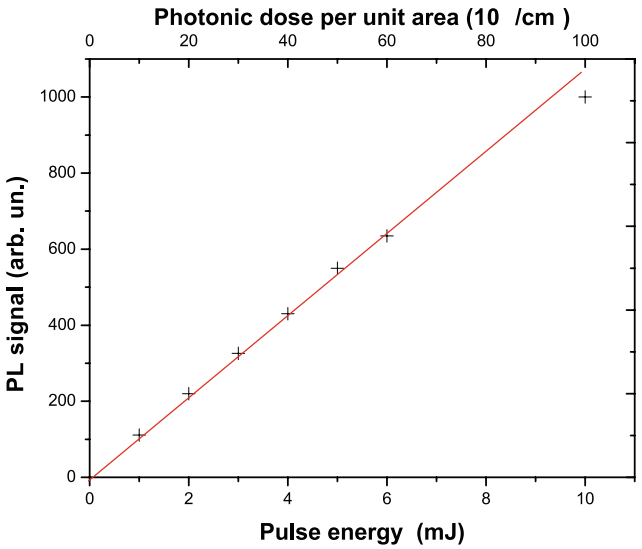

Fig. 6 Dependence of the PL signal on the incident pulse energy, for LN:Fe 0.02% mol at 4 K

Table 4 Radiative lifetime, activation energy and quenching temperature determined by least-square fits of the PL decay time versus temperature, according to (4)

Sample	τ_R (µs)	E_a (meV)	T_Q (K)
LN:Fe 0.02% mol	8.30	205 ± 20	202 ± 20
LN:Fe 0.05% mol	8.12	197 ± 20	194 ± 20
LN:Fe 1% mol	7.98	182 ± 20	176 ± 20

lifetime τ_R and a thermally activated, nonradiative lifetime $\tau_{NR} = \tau_0 \exp(E_a/k_B T)$. The PL quantum efficiency thus varies with temperature according to the law

$$\eta(T) = \frac{\tau(T)}{\tau_R} = \frac{1}{1 + C \times \exp(-E_a/k_B T)}, \quad (5)$$

with $C = \tau_0/\tau_R$. This gives a physical justification to the fitting (1). The influence of the pulse energy W_p on the magnitude of the PL signal was also investigated. W_p was varied from 0.5 to 10 mJ. The results are shown in Fig. 6 for the sample LN:Fe 0.02% mol. The pulse energy is converted into the photonic dose per unit area on the upper horizontal axis, by taking account of the photon energy and the area of the incident spot ($\sim$0.27 mm^2). Contrary to the results of CW measurements (Sect. 3.1.2), the dependence is here linear in the whole range studied.

4 Discussion

Since all iron-doped samples studied herein exhibit similar PL characteristics as a function of temperature (radiative and nonradiative lifetimes, activation energy, quenching temperature), and since these characteristics do not largely differ from those of nominally pure samples, it can be concluded that iron doping has only little influence on the thermokinetics of the PL process. On another hand, the spectral characteristics of the PL band, similar to the light-induced absorption band of bound polarons but slightly shifted to longer wavelengths, do not leave any ambiguity on the nature of the intrinsic defect involved. The fact that this PL band vanishes in stoichiometric LN [15] and in compensated LN:Mg 6% mol [14] definitely confirms that the niobium antisite defect Nb_{Li}, or otherwise a complex defect including Nb_{Li}, is responsible for the PL process.

As concerns the dependence of the PL signal on the incident light intensity, the quadratic regime evidenced at low intensities in LN:Fe 1% mol (and probably also in LN:Fe 0.05% mol and LN:Fe 0.02% mol) suggests that polaron excitation in LN:Fe proceeds in two steps: a first photon transfers an electron from a deep donor Fe^{2+} to a niobium antisite defect, and then a second photon excites this light-induced bound polaron to a metastable state:

$$Fe^{2+} + Nb_{Li}^{5+} \xrightarrow{h\nu} Fe^{3+} + Nb_{Li}^{4+}, \quad (6)$$

$$Nb_{Li}^{4+} + h\nu \rightarrow (Nb^{4+})^*. \quad (7)$$

At low intensity, the polaron has time to relax down to its ground state and then back to a deep trap Fe^{3+}, before the next two incident photons generate a new excitation. The dependence is thus quadratic. The linear regime is reached when the first step of the excitation—i.e. the light-induced electronic transfer from iron to niobium antisite—is saturated. According to this sketch, the empirical function (3)

used to fit the experimental results finds a physical justification, and the threshold intensity I_{lin} above which the linear regime settles (2 kW/cm^2 < I_{lin} < 10 kW/cm^2 depending on samples) should correspond to the saturation intensity of polaron-related light-induced absorption (LIA) under CW illumination. Since LIA experiments in LN:Fe have been done only under pulse illumination so far [6, 7, 16], a direct comparison between our PL results and available LIA results is irrelevant. The saturation of LIA under pulse illumination is expected to occur when the photonic dose per unit area exceeds the reciprocal of the absorption cross section of the deep donor. Accordingly, the corresponding peak intensity ensuring LIA saturation under nanosecond pulses is of course much higher than I_{lin}. Nevertheless, I_{lin} should be proportional to the reciprocal of the average relaxation time of LIA, τ_{LIA}^{-1}, and both should increase with the iron doping level—more precisely with the concentration of Fe^{3+} traps. Our PL results (see Table 3) and previous LIA results [6, 7] clearly evidence this tendency, but quantitative relationships between I_{lin}, τ_{LIA} and [Fe^{3+}] are still missing. This point will be addressed in a forthcoming paper.

The fully linear dependence of the PL signal on the pulse energy evidenced in Fig. 6 does not contradict the results of CW measurements. Under pulse illumination, a quadratic dependence should be expected if the photonic dose per unit area was much smaller than the reciprocal of the absorption cross section of the deep center S_{Fe}. At 532 nm, the value of S_{Fe} is 2.16×10^{-18} cm^2 [12]; hence, the threshold value of the linear regime under a pulsed laser can be estimated to be $1/S_{\mathrm{Fe}} \sim 0.46 \times 10^{17}$ photons/cm^2. The sensitivity of the detector used for time-resolved measurements was unfortunately not sufficient to evidence the quadratic regime expected below this threshold.

One can wonder about the physical nature of the polaronic metastable state involved in photoluminescence. The monoexponential decay rules out any distance-dependent process, and the activation energy of the nonradiative lifetime (∼0.2 eV) fairly corresponds to the hopping barrier of the free polaron, Nb_{Nb}^{4+} (Fig. 7). The excitation to the metastable state could thus correspond to the electronic transfer from the niobium antisite Nb_{Li} to a normally occupied niobium site Nb_{Nb} in first-neighbor position. The nonradiative relaxation could be due the thermal migration of the polaron back from Nb_{Nb} to Nb_{Li}. According to this hypothesis, the previous equation (7) should be re-written in this way:

$$Nb_{Li}^{4+} - Nb_{Nb}^{5+} + h\nu \rightarrow Nb_{Li}^{5+} - Nb_{Nb}^{4+}. \quad (8)$$

If one considers the cationic distances in the crystal structure, it is very likely that the normally occupied niobium site to be invoked in (8) is the first-neighbor site located on the same z-axis as the niobium antisite, at a distance $d_{\mathrm{Li-Nb}} \sim 3.01$ Å. The radiative de-excitation should thus

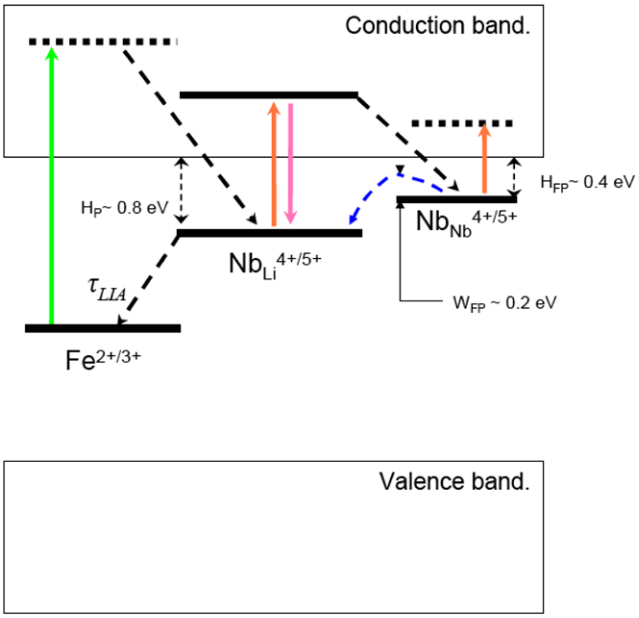

Fig. 7 Schematic energy diagram of excitation and relaxation processes involving the deep level $Fe^{2+/3+}$ and polaron shallow levels $Nb^{4+/5+}$. The energy barrier W_{FP} of the nonradiative relaxation from a free polaron level to a bound polaron level (*dashed curved arrow*) is expected to be one half of the free polaron enthalpy ($W_{\mathrm{FP}} \sim H_{\mathrm{FP}}/2 \sim 0.2$ eV)

correspond to the direct electronic transfer back from Nb_{Nb} to Nb_{Li} in first-neighbor positions. In the LCAO (Linear combination of atomic orbital) approach, the overlapping orbitals of Nb_{Li} and Nb_{Nb} lead to a ionocovalent chemical bond Nb_{Li}–Nb_{Nb}, which can give the so-called bipolaron defect Nb_{Li}^{4+}–Nb_{Nb}^{4+} when two electrons of antiparallel spins are trapped, or otherwise a single bound polaron (either Nb_{Li}^{4+}–Nb_{Nb}^{5+} or Nb_{Li}^{5+}–Nb_{Nb}^{4+}) when only one electron is trapped. We propose that polaron luminescence in lithium niobate is due to excitation and relaxation processes between these two single polaronic states.

It should be stressed that in the linear regime of PL, since the first step of the excitation process schematized by (6) is saturated, the concentration of light-induced bound polarons is equal to the dark concentration of Fe^{2+} donors. Consequently, the magnitude of the PL signal in the linear regime (i.e. the value of the coefficient A that appears in the fitting equation (3) should be proportional to the concentration of deep donors. Our results obtained in LN:Fe 0.02% mol and LN:Fe 0.05% mol confirm this direct proportionality: taking the values of A for these two bulk samples (see Table 3), one obtains the same ratio (∼0.4) as for the corresponding Fe^{2+} concentrations (see Table 1). Since the third sample (LN:Fe 1% mol) is not a bulk one but a doped layer made by Fe diffusion, its gradual Fe^{2+} concentration could not be determined by absorption measurements. Its PL signal collected with a ×100 objective just below the upper surface is logically much stronger than for the two other samples (see

Fig.1). Finally, it can be concluded that polaron luminescence in iron-doped lithium niobate is directly exploitable for measuring the Fe^{2+} concentration. More generally, PL measurements could be used to determine the concentration of any deep donor, provided that its absorption band overlaps with the one of the bound polaron (as is the case for Fe^{2+}) and that the linear regime of PL can be obtained at a convenient exciting wavelength. This method should have a much better sensitivity than conventional techniques, and the major advantage of space resolution at micrometer range.

5 Conclusion

The time decay of polaron photoluminescence in iron-doped lithium niobate follows a classical behavior with temperature. Like undoped lithium niobate, the thermally activated nonradiative relaxation prevails at room temperature, and the radiative process is athermal. Iron doping does not affect significantly any of the parameters (radiative lifetime, activation energy and quenching temperature). On the other hand, the Fe^{2+} concentration and the magnitude of the PL signal seem to show a direct proportionality, which suggests using micro-PL as a powerful tool to detect Fe^{2+} traces ($\leq$1 ppm) at micrometer resolution. As possible outlooks of this work, comparative studies combining several techniques should be done, e.g. combined PL and photovoltaic measurements in thermo-electrically oxidized LN:Fe with low Fe^{2+} content; combined PL and light-induced absorption (LIA) under continuous-wave illumination in reduced highly doped LN:Fe should be useful to clarify the influence of Fe^{3+} concentration on the CW-threshold intensity at which LIA saturates and PL reaches its linear regime.

References

1. L. Arizmendi, Phys. Status Solidi A **201**, 253 (2004)
2. O.F. Schirmer, O. Thiemann, M. Wohlecke, J. Phys. Chem. Solids **52**, 185 (1991)
3. O.F. Schirmer, S. Juppe, J. Koppitz, Cryst. Lattice Defects Amorph. Mater. **16**, 353 (1987)
4. F. Jermann, M. Simon, R. Böwer, E. Krätzig, O. Schirmer, Ferroelectrics **165**, 319 (1995)
5. F. Jermann, J. Otten, J. Opt. Soc. Am. B **10**, 2085 (1993)
6. D. Berben, K. Buse, S. Wevering, P. Herth, M. Imlau, T. Woike, J. Appl. Phys. **87**, 1034 (2000)
7. P. Herth, D. Schaniel, T. Woike, T. Granzow, M. Imlau, E. Krätzig, Phys. Rev. B **71**, 125128 (2005)
8. J. Carnicero, M. Carrascosa, G. Garcia, F. Agullo-Lopez, Phys. Rev. B **72**, 245108 (2005)
9. Y. Zhang, L. Guilbert, P. Bourson, Appl. Phys. B **78**, 355 (2004)
10. A. Harhira, L. Guilbert, P. Bourson, H. Rinnert, Phys. Status Solidi C **4**, 926 (2007)
11. A. Ridah, P. Bourson, M. Fontana, G. Malovichko, J. Phys. Condens. Matter **9**, 9687 (1997)
12. H. Kurz, E. Krätzig, W. Keune, H. Engelmaann, U. Gonser, B. Dischler, A. Räuber, Appl. Phys. **12**, 355 (1977)
13. E. Krätzig, O. Schirmer, Photorefractive centers in electro-optic crystals, in *Photorefractive Materials and Their Applications I*, ed. by P. Günter, J. Huignard (Springer, Berlin, 1988), pp. 131–166
14. B. Faust, H. Müller, O.F. Schirmer, Ferroelectrics **153**, 297 (1994)
15. S.M. Kostritskii, O.G. Sevostyanov, P. Bourson, M. Aillerie, M.D. Fontana, D. Kip, Ferroelectrics **352**, 61 (2007)
16. O. Beyer, D. Maxein, T. Woike, K. Buse, Appl. Phys. B **83**, 527 (2006)